

02,12

Ac susceptibility of the superconducting porous glass/Ga–In–Sn nanocomposite

© O.D. Shevtsova¹, M.V. Likholetova¹, E.V. Charnaya¹, E.V. Shevchenko¹, Yu.A. Kumzerov², A.V. Fokin²

¹ St. Petersburg State University,
St. Petersburg, Russia

² Ioffe Institute,
St. Petersburg, Russia

E-mail: ezhi9327@gmail.com

Received August 30, 2021

Revised August 30, 2021

Accepted September 3, 2021

Interest to studies of gallium alloys increased recently in relation to their prospective applications for self-healing superconducting connections and wires. Special attention is focused on superconductive properties of nanostructured alloys. In the present work we studied the ac susceptibility of a porous glass/Ga–In–Sn nanocomposite within the temperature range from 1.9 to 8 K at bias fields up to 5 T. Two superconducting phase transitions were revealed with temperatures of 5.6 and 3.1 K. Phase diagrams were created. Positive curvature of the parts of critical lines was demonstrated and treated within the framework of a proximity effect model. Vortex activation barriers were found from shifts of the maxima of the imaginary parts of susceptibility with changing the ac frequency. A bend was shown on the field dependence of the activation barriers.

Keywords: Ga–In–Sn triple alloy, nanocomposite, superconductivity, magnetometry.

DOI: 10.21883/PSS.2022.01.52486.195

1. Introduction

At present, studies of superconductivity in nanostructured systems attract profound interest. The attained progress in this area has caused considerable advances both in the application area and in the fundamental physics [1,2]. Significant efforts focus on the issue of creation of nanosuperconductors having different morphology, which makes it possible to affect superconducting properties. One of the possibilities to change the superconductor morphology is the use of solid mesoporous matrices, into which superconducting materials are injected by various methods [3,4]. Such materials include, for instance, silicate porous glasses, zeolites, asbestos and opals. The use of porous matrices having different pore network geometry allows for varying the shape of superconducting inclusions and their mutual location. Thereat, superconductors' typical dimensions due to nanoconfinement can decrease below the coherence length and depth of magnetic field penetration in the corresponding three-dimensional materials. The dendritic shape of superconductive inclusions is implemented in nanoconfinement conditions [5–8], which is a complex problem for other technologies due to fragility issues.

The recent studies of nanocomposites based on porous matrices filled with superconducting metals have revealed a number of common regularities on the background of individual differences, related to pore dimension, links in the superconducting phase and morphology of superconducting inclusions [5–12]. Nanoconfinement causes a change in the superconductivity type due to decrease of coherence length, as well as an increase in values of the upper

critical field and critical current. Nanoconfinement may enhance metals' tendency to polymorphism, accompanied with the occurrence of several superconducting transition temperatures for gallium in opals and porous glasses. On the other hand, the presence of strong and weak Josephson links in a nanocomposite may also be responsible for the stepped pattern of the superconducting transition. For metals, similar phase diagrams were observed in identical opal matrices. The temperature dependences of the critical fields in many cases had positive and negative curvature areas. The dynamic susceptibility studies have revealed a complex dependence of the activation energy of motion of superconducting vortices on constant magnetic field. A more complex configuration of the superconducting phase in eutectic metal alloys may cause new effects as compared to nanocomposites with pure metal inclusions. However, such studies have been carried out only for a binary eutectic alloy Ga–Ag [13].

This paper presents the results of a superconductivity study of the nanocomposite consisted of silica porous glass/triple gallium, indium and tin alloy. Ac magnetization was measured at various bias magnetic fields. Gallium alloys, in particular, a binary gallium alloy with indium and a triple gallium alloy with indium and tin, arouse profound interest in relation to the prospects of use in various modern areas, such as robotics and microelectronics. The Ga–In–Sn triple alloy and a similar alloy with a small addition of other elements (galinstan) are considered as promising materials for superconducting contacts and wires [14,15] due to the recoverability after heating to room

temperature. Superconductivity in the Ga–In–Sn bulk alloy having a composition, close to an eutectic point, was studied in the paper [16]. The superconducting properties of Ga–In–Sn nanodroplets having the average diameter of 110 nm and a different component ratio were studied in [17]. A superconducting transition in a bulk alloy with eutectic composition was observed at 6 K, while the maximum temperature of superconducting transition for nanodroplets reached 6.6 K.

2. Experiment

Porous glass used as a templet was obtained from sodium-borate silicate glass by liquation and leaching. The average size of pores according to nitrogen porosimetry data was equal to 7 nm. The Ga–In–Sn triple alloy was embedded into pores at room temperature under a pressure up to 10 kBar. The alloy composition was close to the eutectic one: 77.2 at.% Ga, 14.4 at.% In, and 8.4 at.% Sn [18]. The bulk alloy melting temperature at the eutectic point is equal to 283.7 K [18], so that the alloy is liquid at room temperature. Pore filling was about 80% according to estimates of porous glass weight before and after filling. The sample under study was cut out from a filled matrix and was thoroughly cleaned from the bulk alloy on the surface. The sample weight was equal to 24.25 mg.

Complex *ac* magnetization was measured on the PPMS-9+EverCool-II unit manufactured by Quantum Design. Temperature dependences of magnetization were obtained in the cooling mode with application of various bias magnetic fields at different frequencies and with different alternating field amplitudes. Temperature varied from 1.9 to 8 K.

3. Results and discussion

The temperature dependences of the real χ' and imaginary χ'' parts of *ac* susceptibility, obtained with application of various bias magnetic fields, are shown in Fig. 1. Measurements were performed at the frequency of 5.01 kHz. Alternating field amplitude was 2 Oe. The susceptibility curves in magnetic fields up to 10 kOe show two steps for χ' and two peaks for χ'' . Both steps on the real part of susceptibility are not sharp even in the low field of 10 Oe. As the bias field increases, the steps and peaks move towards low temperatures, so that only one step on the curve $\chi'(T)$ is observed in fields greater than 10 kOe. To characterize superconductivity in the studied nanocomposite, we introduced four temperatures into the consideration, using the data in Fig. 1. Temperature T_c characterizes the onset of the superconducting state. We calculated it as a temperature at which the first-order derivative of the real part of susceptibility by temperature was equal to 2% of its maximum value. We characterized

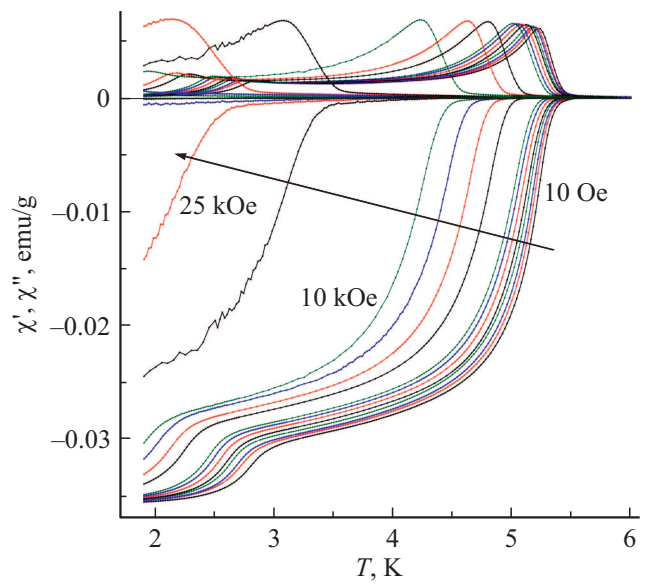


Figure 1. Temperature dependences of the real (bottom) and imaginary (top) parts of susceptibility χ , measured in bias fields 10, 50, 100, 200, 300, 500, 750 Oe and 1, 3, 5, 7.5, 10, 20, 25, 30, 40 kOe. The arrow shows a field increase. Field magnitudes are specified near the three dependences for illustration purposes.

the second, low-temperature, step on the real part of susceptibility by introducing temperature T'_c , at which the first-order derivative increased below the local minimum located directly above the second step, at 0.5%. Temperatures T_p and T'_p show the positions of the maxima of the imaginary part of susceptibility for the first (high-temperature) and second (low-temperature) peaks, respectively. Dependences of these four temperatures on bias field are shown in the phase diagram in Fig. 2.

According to Figs. 1 and 2, superconducting transition temperature for the Ga–In–Sn nanostructured alloy of eutectic composition is equal to $T_c(0) = 5.6$ K. This temperature is significantly higher than the superconductivity temperatures for the three components of the alloy (1.08 K for α -Ga, 3.41 K for In and 3.73 K for Sn). It differs from the critical temperature of about 6 K, found for a bulk triple alloy with the component ratio of 78:15:7 in paper [16]. Superconductivity temperature in the studied nanocomposite is also lower than the maximum transition temperature of 6.6 K, found for the bulk triple alloy of Ga–In–Sn and nanodroplets of the particular composition [17]. Recent studies of the crystalline phase in the Ga–In–Sn bulk alloy [16] have demonstrated the formation of intermetallic compounds of In_3Sn and InSn_4 . Such compounds also form upon crystallization of the In–Sn alloy [19,20]. The In_3Sn compound becomes superconducting at temperatures above 5 K [20]. Thus, it should be supposed that the found superconducting transition temperature is related to the fact that the nanocomposite contains the In_3Sn intermetallic compound, formed upon crystallization of the Ga–In–Sn triple alloy of eutectic composition. The

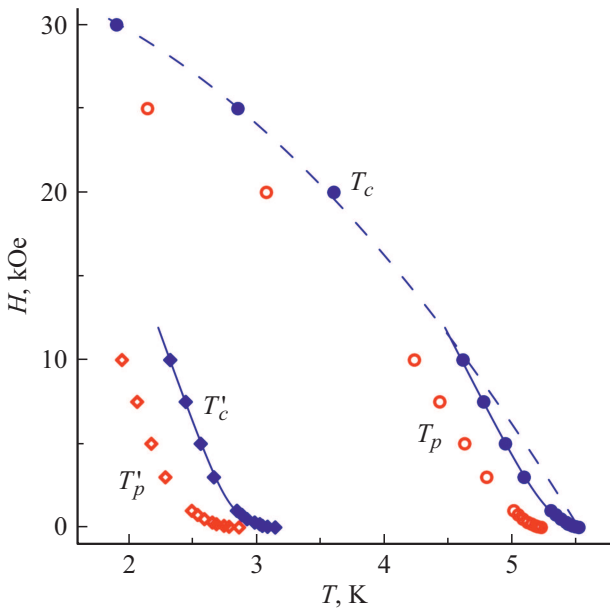


Figure 2. Phase diagram for the first (circles) and second (rhombi) superconducting transitions. Dark symbols are transition temperatures, light symbols are temperatures of the maxima for the imaginary part of susceptibility. Dashed line is the theoretical dependence for the model of two liquids. Solid lines are theoretical curves for the model developed in the paper [23].

low-temperature step on the real part of magnetism is characterized by the temperature of 3.1 K in a zero magnetic field. This temperature is close to the superconductivity temperature of bulk indium. It can be supposed that the second step on the dependence of $\chi'(T)$ is due to the formation of crystalline solid indium solution with a small amount of tin and gallium. It should be noted that the papers [16,17] did not report a second superconducting transition in the Ga–In–Sn triple alloy.

Dependences of the upper critical field on temperature $H_{c2}(T)$ in the phase diagram (Fig. 2) differ from the conventional WHH dependences [21] or a model of two liquids [22], observed for type-II superconductors. Curvature for the first transition is positive in case of low fields and becomes negative at above 10 kOe. Curvature for the second transition remains positive in the whole temperature range of measurements. It should be noted that the $T_p(H)$ dependences also have ranges of anomalous curvature and follow the $H_{c2}(T)$ curves.

The area of the phase diagram for the first transition in the negative curvature region allows for interpretation within the framework of the model of two liquids [22]:

$$H_{c2}(T) = H_{c2}(0) \left[1 - \left(\frac{T}{T_c} \right)^2 \right], \quad (1)$$

at $H_{c2}(0) = 3.38$ kOe. The obtained value of the upper critical field at zero temperature is close to the estimate for the Ga–In–Sn bulk alloy in [16]. According to the Landau

theory, the upper critical field is related to coherence length

$$\xi(0) = \sqrt{\frac{\Phi_0}{2\pi H_{c2}(0)}}, \quad (2)$$

where Φ_0 is the flux quantum. Coherence length in dirty type-II superconductors is limited by the electron free-path length, which depends on spatial inhomogeneity of the superconducting phase [22]. Thus, similarity of critical fields in the Ga–In–Sn bulk alloy and in the studied nanocomposite means an identical inhomogeneity degree of the In_3Sn phase in both cases.

The positive curvature ranges on the $H_{c2}(T)$ dependence allow for interpretation within the framework of the model considered in [23]. The model analyzes the set of irregular superconducting and nonsuperconducting layers linked by a Josephson interaction. The proximity effect conditions the emergence of a non-zero order parameter in nonsuperconducting layers. Spatial variation of the order parameter leads to positive curvature of the critical line near T_c . As the magnetic field increases, the order parameter in nonsuperconducting layers decreases remarkably due to the decreased coherence length and the proximity effect is no longer significant. Figure 2 shows an approximation of the positive curvature areas on critical dependences of $H_{c2}(T)$ using the formula (13) from [23].

Figure 3 shows temperature dependences of the imaginary part of susceptibility, obtained at the frequency of 5.01 kHz at different amplitudes H_{ac} of the alternating field in a zero bias field. It is seen that the positions of the peaks, corresponding to both superconducting transitions, move considerably towards low temperatures as amplitude increases. The insert for Fig. 3 shows that the relation

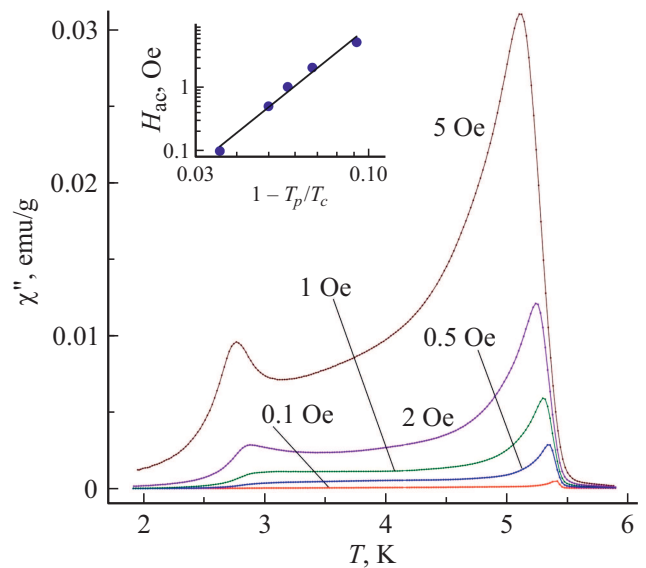


Figure 3. Imaginary part of susceptibility measured at the frequency of 5.01 kHz for the alternating field amplitude of 0.1, 0.5, 1, 2 and 5 Oe. The insert shows dependence of alternating field amplitude H_{ac} on $1 - T_p/T_c$, obtained in a zero bias field.

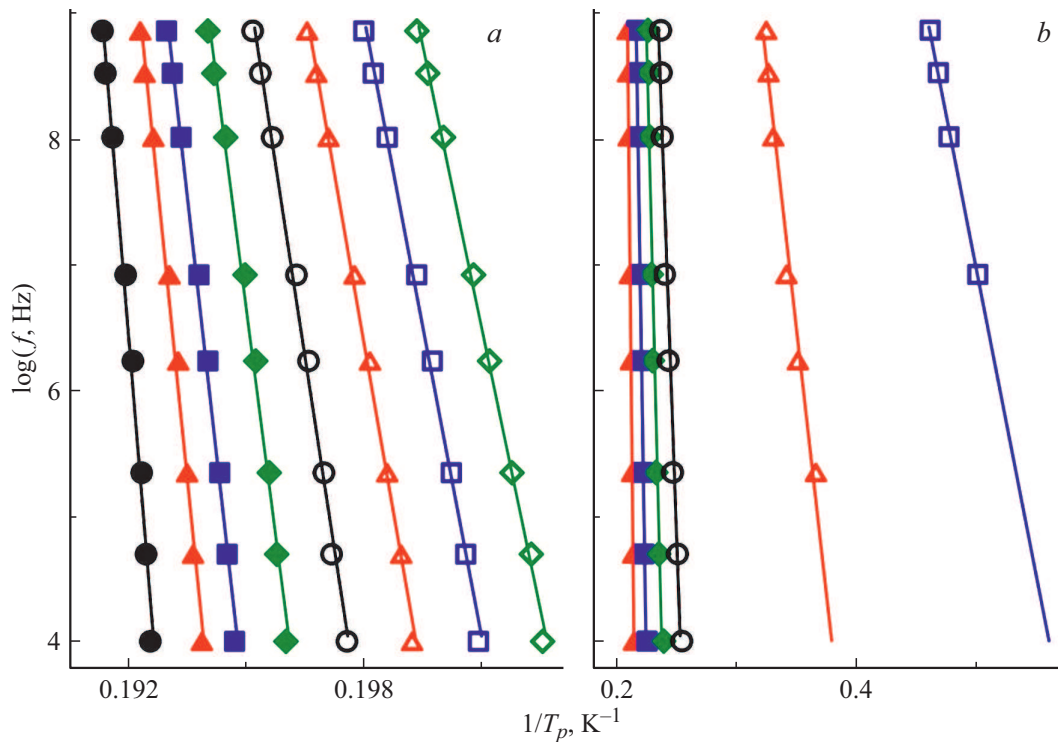


Figure 4. Arrhenius plots for the first superconducting transition obtained in bias fields (from left to right) 10, 50, 100, 200, 300, 500, 750 Oe and 1 kOe (a) and 3, 5, 7.5, 10, 20, 25 kOe (b). Straight lines are linear dependences.

between temperature of the susceptibility maximum T_p and H_{ac} for the first superconducting transition obeys the power law

$$H_{ac} \propto \left(1 - \frac{T_p}{T_c}\right)^\beta. \quad (3)$$

The index β is equal to 4.2. Along with a strong amplitude dependence of the peak positions, the studies carried out at different alternating field frequencies have revealed weak regular shifts of the peaks of the imaginary part of susceptibility with frequency. A weak change in T_p as frequency changes means a weak dependence of critical current on electric field, as well as the proportionality of critical current to amplitude H_{ac} at temperature T_p [24–26]. Thus, the relation between critical current and T_p is given by an expression identical to (3). As demonstrated in [9,27,28], a model of granular superconductors where granules are bound by strong or weak Josephson links is applicable to nanocomposites based on mesoporous hard matrices with metallic inclusions. Thereat, the granules consist of several neighboring pores connected by filled channels [6,28,29]. According to [30] the exponent in formula (3) is equal to 3/2 for strongly linked granules and decreases for weak linked. The exponent for the nanocomposite under study is considerably greater, which requires an additional theoretical analysis. A similar result was obtained for porous glass filled with Ga–Ag alloy [13]. For the second superconducting transition, the available data is insufficient for approximation of the relation between T_p and H_{ac} .

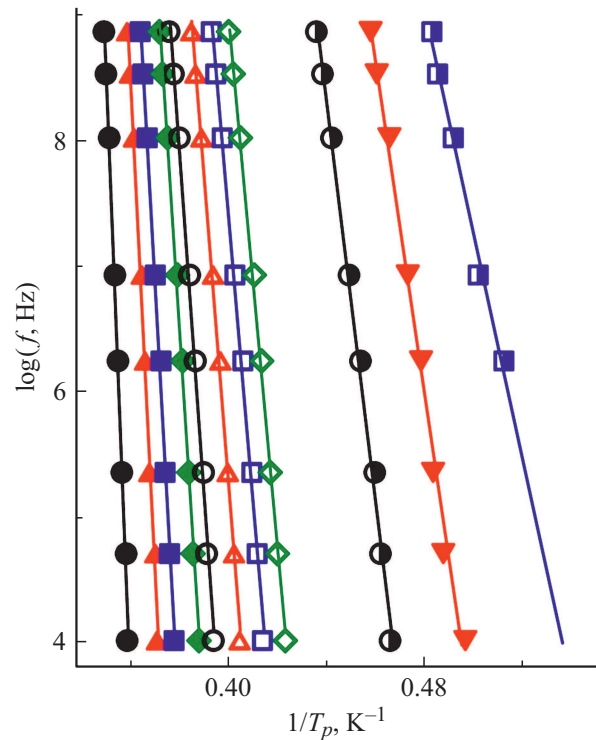


Figure 5. Arrhenius plots for the second superconducting transition obtained in bias fields (from left to right) 10, 50, 100, 200, 300, 500, 750 Oe and 1, 3, 5, 7.5 kOe. Straight lines are linear dependences.

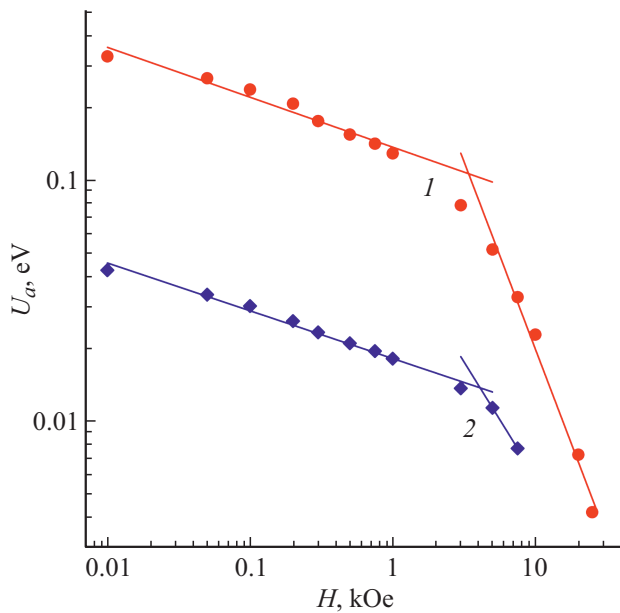


Figure 6. Dependence of activation barriers on bias field for the first (1) and second (2) superconducting transitions. Straight lines are power-law dependences.

Strong influence of alternating field amplitude on the value of T_p and weak dependence of T_p on frequency mean the thermoactivation nature of motion of superconducting vortices [22,31–33]. The peak offsets are considerable enough to construct Arrhenius plots. These plots for the alternating field amplitude of 2 Oe are given in Fig. 4 for the first transition and in Fig. 5 for the second transition. Figures 4 and 5 demonstrate linear dependences of the frequency logarithm on reciprocal temperature of the maximum values of the susceptibility imaginary part for both superconducting transitions, making it possible to calculate activation barriers U_a . The activation barrier values for different bias fields are given in Fig. 6.

Two areas can be distinguished for the first and second superconducting transitions on the dependences of activation barriers on bias field. Activation barriers on both areas change as the field changes, following the power law $U_a \propto H^{-\alpha}$. Power exponent α in fields up to 3 kOe is significantly less than one, which reflects the weak dependence of U_a on field ($\alpha = 0.21$ for the first transition and $\alpha = 0.20$ for the second transition). Above 5 kOe, the dependence of activation barriers on field becomes much stronger and the exponent increases to 1.56 and 0.96 for the first and second transitions, respectively. Bends on the field dependence of activation barriers were observed for different type-II superconductors, e.g., for unconventional superconductors (see [34–36] and references in these papers), as well as for nanocomposites with inclusions of a number of pure metals and the gallium alloy with silver [5,11,13]. The found bends were interpreted on the basis of various models, in particular, as a manifestation of a phase transition in the vortex system. For the composite under study, a transformation

in the vortex system upon increasing field can be related to the redistribution of vortices in space between granules and inside granules [11]. The nanocomposite behaves in small fields as a dirty type-II superconductor. Vortices are pinned on irregularities between granules. When moving to other pinning centers, vortices cross high potential barriers. Field enhancement causes gradual breaking of links between superconducting granules and transition of intergranular areas to the normal state. Vortex mobility is limited by granule sizes. Activation barriers become smaller due to greater homogeneity of granules, which causes a bend on the field dependence of U_a . In papers [11,13] the fields at which a bend was observed were close to fields of crossover from the positive to negative curvature of the critical line. However, in case of the nanocomposite with the Ga–In–Sn triple alloy studied here, the magnetic fields corresponding to bend and crossover do not correlate with each other. Within the model framework [23], a crossover field is defined by field dependence of the proximity effect influenced by nanocomposite morphology. Thus, it should be supposed that the morphology of the porous glass/Ga–In–Sn composite differs from the morphology of the nanocomposites studied in papers [11,13].

4. Conclusion

The studies of ac susceptibility for the nanocomposite of porous glass/eutectic Ga–In–Sn alloy have revealed a two-stage superconducting transition with the characteristic temperatures of 5.6 and 3.1 K. These temperatures are supposedly related to the formation of an intermetallic In_3Sn compound and solid indium solution with a small amount of gallium and stannum in pores. The dependences of the upper critical field on temperature have positive curvature areas and allow for interpretation based on a model that takes into account the proximity effect. The strong amplitude and weak frequency dependences of the imaginary part of susceptibility mean an activation nature of vortex motion. The calculated activation barriers vary as bias fields change following the power law. Thereat, the exponent increases significantly in strong fields.

Funding

The research was funded by Russian Scientific Foundation (grant 21-72-20038). The measurements were performed using the equipment of the Resource Center of the „Centre for Diagnostics of Functional Materials for Medicine, Pharmacology and Nanoelectronics“ of the Saint Petersburg State University Research Park.

Conflict of interest

The authors declare that they have no conflict of interest.

References

- [1] The Oxford handbook of small superconductors / Ed. A.V. Narlikar. Oxford University Press, Oxford (2017).
- [2] Superconductors at the nanoscale. From basic research to applications / Ed. R. Wördenweber, V. Moshchalkov, S. Bending, F. Tafuri. eBook De Gruyter (2017).
- [3] Y. Kumzerov, S. Vakhrushev. In: Encyclopedia of Nanoscience and Nanotechnology / Ed. H.S. Nalwa. American Scientific Publishers (2004). V. 7. P. 811.
- [4] M. Salvato, R. Baghdadi, C. Cirillo, S.L. Prischepa, A.L. Dolgiy, V.P. Bondarenko, F. Lombardi, C. Attanasio. *Nanotechnology* **28**, 465301 (2017).
- [5] M.K. Lee, E.V. Charnaya, C. Tien, L.J. Chang, Y.A. Kumzerov, *J. Appl. Phys.* **113**, 113903 (2013).
- [6] E.V. Charnaya, C. Tien, K.J. Lin, Y.A. Kumzerov. *Phys. Rev. B* **58**, 11089 (1998).
- [7] E.V. Charnaya, C. Tien, M.K. Lee, Y.A. Kumzerov. *J. Phys.: Condens. Matter* **21**, 455304 (2009).
- [8] M.K. Lee, C. Tien, E.V. Charnaya, H.-S. Sheu, Y.A. Kumzerov. *Phys. Lett. A* **374**, 1570 (2010).
- [9] Y.S. Ciou, M.K. Lee, E.V. Charnaya, C. Tien, L.J. Chang, Y.A. Kumzerov, M.I. Samoylovich. *Supercond. Sci. Technol.* **26**, 055009 (2013).
- [10] C. Tien, E.V. Charnaya, D.Y. Xing, A.L. Pirozerskii, Y.A. Kumzerov, Y.S. Ciou, M.K. Lee. *Phys. Rev. B* **83**, 014502 (2011).
- [11] M.K. Lee, E.V. Charnaya, S. Mühlbauer, U. Jeng, L.J. Chang, Y.A. Kumzerov. *Sci. Rep.* **11**, 4807 (2021).
- [12] D.Yu. Nefedov, E.V. Charnaya, A.V. Uskov, A.O. Antonenko, D.Yu. Podorozhkin, J. Haase, Y.A. Kumzerov, A.V. Fokin. *Appl. Magn. Res.* (2021). Published online. DOI 10.1007/s00723-021-01385-4.
- [13] E.V. Shevchenko, E.V. Charnaya, M.K. Lee, L.-J. Chang, M.V. Likholetova, I.E. Lezova, Y.A. Kumzerov, A.V. Fokin. *Physica C* **574**, 1353666 (2020).
- [14] N. Ochirkhuyag, R. Matsuda, Z. Song, F. Nakamura, T. Endo, H. Ota. *Nanoscale* **13**, 2113 (2021).
- [15] G. Bo, L. Ren, X. Xu, Y. Du, S. Dou. *Adv. Phys. X* **3**, 1446359 (2018).
- [16] T. Mochiku, M. Tachiki, S. Ooi, Y. Matsushita. *Physica C* **263**, 33 (2019).
- [17] L. Ren, J. Zhuang, G. Casillas, H. Feng, Y. Liu, X. Xu, Y. Liu, J. Chen, Y. Du, L. Jiang, S.X. Dou. *Adv. Func. Mater.* **26**, 8111 (2016).
- [18] Y. Plevachuk, V. Sklyarchuk, S. Eckert, G. Gerbeth, R. Novakovic. *J. Chem. Eng. Data* **59**, 757 (2014).
- [19] Y. Shu, T. Ando, Q. Yin, G. Zhou, Z. Gu. *Nanoscale* **9**, 12398 (2017).
- [20] M.F. Merriam, M. Von Herzeni. *Phys. Rev.* **131**, 637 (1963).
- [21] N.R. Werthamer, E. Helfand, P.C. Hohenberg. *Phys. Rev.* **147**, 295 (1966).
- [22] Tinkham M. *Introduction to Superconductivity*. 2 nd.ed. Dover Publications (2004).
- [23] S. Theodorakis, Z. Teanovic. *Phys. Rev. B* **40**, 6659 (1989).
- [24] E.H. Brandt. *Phys. Rev. B* **55**, 14513 (1997).
- [25] F. Gömöry. *Supercond. Sci. Technol.* **10**, 523 (1997).
- [26] J.R. Clem, A. Sanchez. *Phys. Rev. B* **50**, 9355 (1994).
- [27] E.V. Charnaya, C. Tien, K.J. Lin, C.-S. Wur, Y.A. Kumzerov. *Phys. Rev. B* **58**, 467 (1998).
- [28] E.V. Charnaya, C. Tien, C. S. Wur, Y.A. Kumzerov. *Physica C* **269**, 313 (1996).
- [29] E.V. Charnaya, C. Tien, M.K. Lee, Y.A. Kumzerov. In: *Indium: Properties, Technological Applications and Health Issues* (2013). P. 1.
- [30] J.R. Clem, B. Bumble, S.I. Raider, W.J. Gallagher, Y.C. Shih. *Phys. Rev. B* **35**, 6637 (1987).
- [31] T.T.M. Palstra, B. Batlogg, R.B. van Dover, L.F. Schneemeyer, J.V. Waszczak. *Phys. Rev. B* **41**, 6621 (1990).
- [32] P.W. Anderson, Y.B. Kim. *Rev. Mod. Phys.* **36**, 39 (1964).
- [33] G. Prando, P. Carretta, R. De Renzi, S. Sanna, A. Palenzona, M. Putti, M. Tropeano. *Phys. Rev. B* **83**, 174514 (2011).
- [34] G. Prando, P. Carretta, R. De Renzi, S. Sanna, H.-J. Grafe, S. Wurmehl, B. Büchner. *Phys. Rev. B* **85**, 144522 (2012).
- [35] S.R. Ghorbani, X.L. Wang, M. Shabazi, S.X. Dou, K.Y. Choi, C.T. Lin. *Appl. Phys. Lett.* **100**, 072603 (2012).
- [36] H. Lei, R. Hu, C. Petrovic. *Phys. Rev. B* **84**, 014520 (2011).